




Static bending and vibration analysis of piezoelectric semiconductor beams considering surface effects

Zhicheng Zhang¹ · Chao Liang² · Yun Wang³ · Rongqiao Xu¹ · Cunfa Gao⁴ · Chunli Zhang² 

Received: 14 February 2021 / Revised: 27 April 2021 / Accepted: 24 May 2021 / Published online: 31 May 2021
© Krishtel eMaging Solutions Private Limited 2021, corrected publication 2021

Abstract

Based on the surface elasticity theory established by Gurtin and Murdoch, one-dimensional (1D) multi-field coupling model incorporating surface effects for piezoelectric semiconductor (PS) nanostructures is developed, in which the surface effect is treated as a non-classical mechanical boundary condition. With the derived equations, we conduct a theoretical analysis of static bending and free vibration of a simply supported n-type PS beam with open-circuit and electrically isolated boundary conditions at two ends. Numerical results show that the surface effect can stiffen the PS beam, and thus enhance its natural frequencies. Due to the influence of surface effects, the physical quantities such as the effective rigidity and natural frequencies of the PS beam exhibit a considerably significant size-dependent property when the radius R of the PS beam's cross-section is smaller than 400 nm. For the free vibration of the PS beam, the motion of electrons causes a damping effect. Both the surface effect and initial concentration of electrons have an effect on the quasi-damping ratio of the PS beam. The surface effect tends to enhance the damping effect.

Keywords PS beams · Piezotronics · Surface effects · Bending · Vibration

Introduction

Traditional semiconductors without piezoelectricity such as silicon materials lay the foundation for modern electronics industry and the information age. The third-generation (3G) semiconductors, including ZnO, GaN, and AlN to name but a few, possess both semiconductor properties and piezoelectricity and are also known as piezoelectric semiconductors (PSs). In which the interaction between piezoelectricity and semiconductor behaviors leads to the appearance of piezotronic effects. The key physical mechanism of the

piezotronic effect is the stress- (or strain) induced polarization acting as a “gate” voltage to adjust the transport behavior of carriers across a PS interface or junction [1–4]. It makes PSs a very promising application in multi-functional sensors and actuators which are crucial to the Internet of Things and Artificial Intelligence age. In recent decades, some researchers have fabricated a lot of low-dimensional PS materials and structures such as one-dimensional (1D) fibers/tubes/belts/spirals, and two-dimensional (2D) film-type PS structures [5] with good physical and mechanical properties, and used them to make nanogenerators [6–8], field-effect transistors [9, 10], and strain [11, 12]/gas [13, 14]/humidity [15]/chemical [16] sensors.

The prediction of multi-filed coupling behaviors of PSs is of fundamental importance for practical applications of multi-functional PS devices. In recent years, several researchers have conducted insightful theoretical studies on static extension/compression/bending of ZnO rods under different conditions [17–20], free vibration behaviors of ZnO rods [21, 22], and extensional vibrations of ZnO rods [23, 24]. In view of many fiber-based devices [7, 8] usually operating under compression, Liang et al. [25] investigated the static buckling response of a ZnO nanofiber with different boundary conditions with

✉ Chunli Zhang
zhangcl01@zju.edu.cn

¹ Department of Civil Engineering, Zhejiang University, Hangzhou 310058, China

² Key Laboratory of Soft Machines and Smart Devices of Zhejiang Province, Department of Engineering Mechanics, Zhejiang University, Hangzhou 310027, China

³ School of Mechanical Engineering, Hangzhou Dianzi University, Hangzhou 310018, China

⁴ State Key Laboratory of Mechanics and Control of Mechanical Structures, Nanjing University of Aeronautics and Astronautics, Nanjing 210016, China

considering full deformation-polarization-carrier coupling. The analytical expressions of critical forces and stresses, depending on the geometrical aspect, boundary condition, material property, and carrier concentration of the considered PS rod, were presented in Ref. [25], as well. Interestingly, a local load such as a local mechanical force [26] or local temperature change [27] can lead to the formation of local barriers and wells in a single n-type ZnO fiber. This provides a new approach to making an electrical on-off switch device with a single n-/p-type PS structure instead of traditional p-n junction or Schottky contact structures. With the concept of composite material, Cheng et al. [28] and Luo et al. [29] proposed a 2–2 type of laminated PS composite structure consisting of both piezoelectric and semiconductor layers, in which the piezotronic effect is theoretically demonstrated. Furthermore, Cheng et al. [30] realized magnetically controlling of piezotronic effects via a laminated piezomagnetic/PS/piezomagnetic composite structure. In addition, some researchers have also studied crack problems [31–33] and wave propagation [34–36] in PSs.

For a solid or crystal, the physical properties of the surface are quite different from those of the bulk. However, at macroscopic scale, such a difference brings a very tiny effect to the entire behavior of solids, and is thus negligible. At nanoscale, the surface plays a substantial role in multi-field coupling responses of a solid. For example, Chen et al. [37] experimentally found the size dependence of Young's modulus for ZnO wires, at the same time that for ZnO films was shown in Ref. [38] by atomistic simulations. With the help of the knowledge of differential geometric, Gurtin and Murdoch [39, 40] originally developed a rigorous elastic surface theory within the framework of continuum mechanics, also known as the G-M theory. In the spirit of the G-M theory, a solid includes one three-dimensional (3D) bulk part and the other enclosed two-dimensional material surface part without thickness. Both the surface stress and inertia of the surface part give a traction on the bulk. From the view of equilibrium of the bulk part, the surface effect is identified with a non-classical boundary condition. Based on the G-M theory, researchers have investigated the size-dependent property of macroscopic responses of elastic ultra-thin structures [41, 42], and the influence of surface effects on an isotropic elastic half-space [43]. The G-M theory is also extended to study mechanical behaviors of piezoelectric materials and structures [44–51]. For instance, researchers studied the effect of surface effects on the electromechanical coupling of piezoelectric rings [44] and fibers [48, 49], the buckling behavior [50, 51] of piezoelectric fibers, and on the contact response of a piezoelectric half-plane [45]. A more

generalized structural theory for piezoelectric structures incorporating surface effects was systematically developed in Refs. [46, 47]. It should be mentioned that the nonlocal theory [52, 53] can be also used to investigate macroscopic behaviors of nanostructures.

Similarly, surface effects have to play a significant role in the performance of PS devices at nanoscale. The understanding of how the surface effect influences multi-field coupling behaviors of PS nanostructures is fundamental to the development of PS devices. However, to the authors' knowledge, there is no relevant theoretical study yet. In this paper, based on the G-M theory, we develop the 1D theoretical model for PSs, appropriate to the analysis of PS nanowires/fibers/rods/beams, by taking the surface effect and full deformation-polarization-carrier coupling into consideration. In doing so, we divide a PS structure into two parts, i.e., of the bulk core and the surface without thickness. The surface effect is treated as the non-classical mechanical boundary condition on the bulk core. With the derived equations, the static bending and free vibration of a simply supported n-type PS beam are investigated. The analytical solutions for displacement, electric potential, and concentration of carriers in the considered PS beam are presented, and the surface effect on the static and free vibration responses are examined as well. The paper is organized as follows. In Sect. 2, the 3D basic equations for PSs and the surface equations for piezoelectric materials are summarized. Based on them, the 1D theoretical model is developed for PSs incorporating surface effects in Sect. 3. Thereupon, the static bending of a simply supported PS beam is studied in Sect. 4, and the free vibration analysis is conducted in Sect. 5. Some numerical results and discussion are provided in Sect. 6. Finally, some conclusions are drawn in Sect. 7.

Basic equations

First briefly summarize the 3D equations of PSs for the bulk part. For a doped PS solid with donors N_D^+ and acceptors N_A^- , its multi-field coupling behavior can be described by the linear theory of piezoelectricity and semiconductor equations for carriers [54, 55]. The basic physical quantities include displacements u_i , strains S_{ij} , stresses T_{ij} , electric potential φ , electric fields E_i , electric displacements D_i , hole and electron concentrations p and n , hole and electron current densities J_i^p and J_i^n . The constitutive relations of stresses and electric displacements read

$$\begin{aligned} T_{ij} &= c_{ijkl}S_{kl} - e_{kij}E_k, \\ D_i &= e_{ikl}S_{kl} + \varepsilon_{ik}E_k, \end{aligned} \quad (1)$$

where c_{ijkl} , e_{kij} , and ϵ_{ij} are the elastic, piezoelectric, and dielectric constants, respectively. The strain and electric field components are related to u_i and ϕ , respectively

$$S_{ij} = \frac{1}{2}(u_{i,j} + u_{j,i}), \quad E_i = -\phi_{,i}. \tag{2}$$

The hole and electron currents include the drift current the flow of carriers in response to the electric field, and the diffusion current produced by non-uniform distribution of carriers. As the drift current is nonlinear, leading to considerable difficulty in obtaining an analytical solution to the problem, a linearized method is proposed in [19, 56]. In which the hole and electron concentrations are written as $p = p_0 + \Delta p$ and $n = n_0 + \Delta n$, respectively. p_0 and n_0 represent initial concentrations of holes and electrons, Δp and Δn denote perturbations of holes and electrons which are far smaller than p and n , respectively. In this sense, for a uniform-doped PS with $n_0 = N_D^+$ and $p_0 = N_A^-$, the linear constitutive relations of hole and electron current densities can be written as

$$\begin{aligned} J_i^p &= qp_0\mu_{ij}^p E_j - qD_{ij}^p \Delta p_{,j}, \\ J_i^n &= qn_0\mu_{ij}^n E_j + qD_{ij}^n \Delta n_{,j}. \end{aligned} \tag{3}$$

In Eq. (3), μ_{ij}^p and μ_{ij}^n are the mobility of holes and electrons, and D_{ij}^p and D_{ij}^n the diffusion constants of holes and electrons.

For PSs, the equilibrium equations of motion, the charge equation of electrostatics, and the continuity equations for holes and electrons are

$$\begin{aligned} T_{ij,i} &= \rho \ddot{u}_j, \\ D_{i,i} &= q(\Delta p - \Delta n), \\ J_{i,i}^p &= -q \frac{\partial}{\partial t}(\Delta p), \\ J_{i,i}^n &= q \frac{\partial}{\partial t}(\Delta n), \end{aligned} \tag{4}$$

where ρ is material density, and $q = 1.6 \times 10^{-19} \text{C}$ the elementary charge. It can be seen from Eq. (4) that both piezoelectricity and semiconductor properties are coupled together through the charge equation of electrostatics of Eq. (4)₂.

For the surface part, according to the G-M theory, the material properties are different from those of the bulk core. The constitute relations of the surface stress components T_{ab}^s and the electric displacement components D_a^s at the surface, here a and $b \in (1, 3)$, are [44]

$$\begin{aligned} T_{ab}^s &= T_{ab}^0 + c_{abcd}^s S_{cd} - e_{abk}^s E_k, \\ D_a^s &= e_{acd}^s S_{cd} + \epsilon_{ak}^s E_k. \end{aligned} \tag{5}$$

In Eq. (5), T_{ab}^0 denote the surface residual stress components, and c_{abcd}^s , e_{abk}^s , and ϵ_{ak}^s the surface

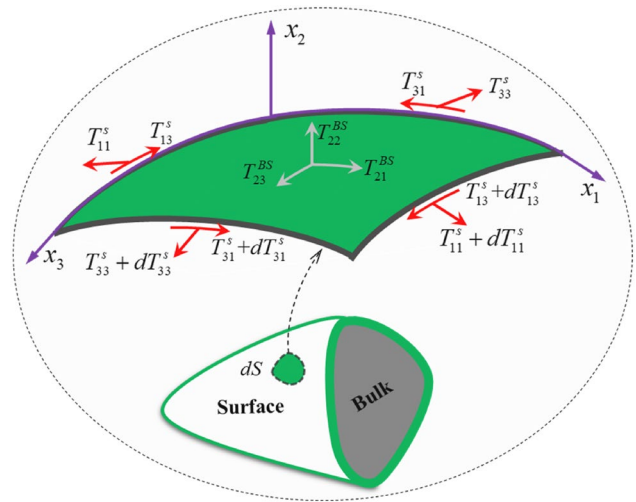


Fig. 1 Sketch of the G-M surface model

elastic, piezoelectric, and dielectric constants, respectively. According to the G-M theory, the surface keeps in its equilibrium state under the action of both T_{ia}^s and T_{i2}^{Bs} , as shown in Fig. 1. Here, T_{i2}^{Bs} are the reaction forces of the bulk core against the surface. The surface equilibrium equation reads

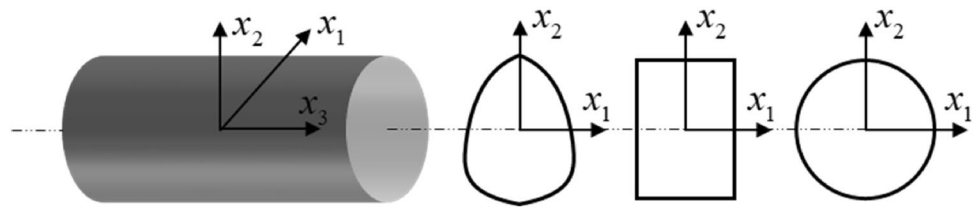
$$T_{ia,a}^s + T_{i2}^{Bs} = \rho^s \ddot{u}_i. \tag{6}$$

Equation (6) is also referred to as the generalized Young–Laplace equation for curved surfaces or interfaces [57]. Equation (6) can be rewritten as an alternative form of $T_{i2}^{Bs} = \rho^s \ddot{u}_i - T_{ia,a}^s$, showing the mechanical nature of the surface effect acting as a non-classical boundary condition. For nanostructures, the surface residual stress also has an effect on their macroscopic behaviors. This mainly depends on the values of the surface residual stress constants T_{ab}^0 , but T_{ab}^0 are difficult to be measured at present. At the same time, our main concern is how the electromechanical coupling of the surface part, which is not included in classical continuum theory, influences macroscopic responses of nanostructures. For convenience, we neglect the effect of the surface residual stress in this paper.

One-dimensional equations of PS beams incorporating surface effects

In this section, we develop the 1D theoretical model for PSs with surface effects, which are appropriate for investigating common extension/compression/flexural/shear deformations of rod- or beam-like structures. Consider an n-type beam-like PS structure with arbitrary cross-section with a

Fig. 2 Sketch of a PS beam with arbitrary cross-section with a symmetrical axis



symmetrical axis as shown in Fig. 2. Its axial line is along with x_3 , and its cross-section locates in the x_1 - x_2 plane. Assume that the length of the considered beam is far larger than its transversal aspects.

As stated in the above, we treat the surface effect of PS beams as a non-classical boundary condition. By integrating the product of the 3D field equations and x_2 over the cross-section for the bulk core, the coordinate variables of x_1 and x_3 can thus be canceled out, and then, the 1D theoretical model for PS beams incorporating surface effects can be obtained. According to [54], the zeroth- and first-order equilibrium equations of motion, charge equations of electrostatics, and continuity equations for electrons are

$$T_{aj,a}^{(0)} + \oint_{\Gamma_s} [T_{lj}^{Bs}] dx_2 - \oint_{\Gamma_s} [T_{2j}^{Bs}] dx_1 = \int_A \rho \ddot{u}_j dA,$$

$$T_{aj,a}^{(1)} - T_{2j}^{(0)} + \oint_{\Gamma_s} [x_2 T_{lj}^{Bs}] dx_2 - \oint_{\Gamma_s} [x_2 T_{2j}^{Bs}] dx_1 = \int_A \rho \ddot{u}_j x_2 dA, \tag{7}$$

$$D_{a,a}^{(0)} + \oint_{\Gamma_s} D_1 dx_2 - \oint_{\Gamma_s} D_2 dx_1 = \int_A q(\Delta p - \Delta n) dA,$$

$$D_{a,a}^{(1)} - D_2^{(0)} + \oint_{\Gamma_s} [x_2 D_1] dx_2 - \oint_{\Gamma_s} [x_2 D_2] dx_1 = \int_A q(\Delta p - \Delta n) x_2 dA, \tag{8}$$

$$J_{a,a}^{n(0)} + \oint_{\Gamma_s} J_1^n dx_2 - \oint_{\Gamma_s} J_2^n dx_1 = \int_A q \Delta \dot{n} dA,$$

$$J_{a,a}^{n(1)} - J_2^{n(0)} + \oint_{\Gamma_s} [x_2 J_1^n] dx_2 - \oint_{\Gamma_s} [x_2 J_2^n] dx_1 = \int_A q x_2 \Delta \dot{n} dA. \tag{9}$$

$T_{aj}^{(0)}$, $D_a^{(0)}$, and $J_a^{n(0)}$ are the zeroth-order stress, electric displacement, and current density components, respectively, and $T_{aj}^{(1)}$, $D_a^{(1)}$, and $J_a^{n(1)}$ represent the corresponding first-order ones. They are given as

$$T_{aj}^{(0)} = \int_A T_{aj} dA, \quad D_a^{(0)} = \int_A D_a dA, \quad J_a^{n(0)} = \int_A J_a^n dA,$$

$$T_{aj}^{(1)} = \int_A x_2 T_{aj} dA, \quad D_a^{(1)} = \int_A x_2 D_a dA, \quad J_a^{n(1)} = \int_A x_2 J_a^n dA. \tag{10}$$

It can be seen that Eq. (7) includes the action of the surface part on the bulk core. Substituting $T_{i2}^{Bs} = \rho^s \ddot{u}_i - T_{ia,a}^s$ into Eq. (7), we can obtain the 1D theoretical model for

PS beams with arbitrary cross-section incorporating surface effects.

Next, we present the 1D basic bending equations for an n-type PS beam with circular cross-section. For the bending PS beam with shear deformation, we assume that the displacements, electric potential, and concentration of incremental electrons have the following approximations [19, 25]: $u_2 \cong v(x_3, t)$, $u_3 \cong x_2 \psi(x_3, t)$, $\phi \cong x_2 \varphi^{(1)}(x_3, t)$, and $\Delta n \cong x_2 n^{(1)}(x_3, t)$. v is the deflection, ψ is the shear deformation accompanying bending. Substituting them into Eqs. (1), (10), and (7), we have

$$Q_{,3}^* = \rho A \dot{v}, \quad M_{,3}^* - Q^* = \rho I \dot{\psi}, \tag{11}$$

where $Q^* = Q^s + Q$ and $M^* = M^s + M$, and

$$M = \bar{c}_{33} I \psi_{,3} + \bar{e}_{33} I \varphi_{,3}^{(1)},$$

$$Q = \bar{c}_{44} A (v_{,3} + \psi) + \bar{e}_{15} A \varphi^{(1)},$$

$$Q^s = [c_{44}^s (v_{,3} + \psi) + e_{15}^s \varphi^{(1)}] \pi R,$$

$$M^s = (c_{33}^s \psi_{,3} + e_{33}^s \varphi_{,3}^{(1)}) I^s. \tag{12}$$

In Eq. (12), $I = \pi R^4/4$ is the moment of inertia, $A = \pi R^2$ the area of the cross-section, and $I^s = \pi R^3$. Q and M are the shear force and bending moment of the buck core. Q^s and M^s can be regarded as the equivalent shear force and bending moment. From Eqs. (8) and (9), we obtain

$$D_{3,3}^{(1)} - D_2^{(0)} = -q I n^{(1)},$$

$$J_{3,3}^{n(1)} - J_2^{n(0)} = q I \dot{n}^{(1)}, \tag{13}$$

where

$$D_2^{(0)} = \bar{e}_{15} A (v_{,3} + \psi) - \bar{e}_{11} A \varphi^{(1)},$$

$$D_3^{(1)} = \bar{e}_{33} I \psi_{,3} - \bar{e}_{33} I \varphi_{,3}^{(1)}, \tag{14}$$

$$J_2^{n(0)} = -q n_0 \mu_{11}^n A \phi^{(1)} + q D_{11}^n A n^{(1)},$$

$$J_3^{n(1)} = -q n_0 \mu_{33}^n I \phi_{,3}^{(1)} + q D_{33}^n I n_{,3}^{(1)}. \tag{15}$$

In Eqs. (12), (14), and (15), the 1D effective material constants are

$$\begin{aligned} \bar{c}_{33} &= 1/s_{33}, \quad \bar{c}_{44} = 1/s_{44}, \quad \bar{e}_{33} = d_{33}/s_{33}, \quad \bar{e}_{15} = d_{15}/s_{44}, \\ \bar{\epsilon}_{11} &= \epsilon_{11} - d_{15}^2/s_{44}, \quad \bar{\epsilon}_{33} = \epsilon_{33} - d_{33}^2/s_{33}. \end{aligned} \tag{16}$$

So far, the generalized 1D bending model for PS beams incorporating surface effects is developed, from which the classical Euler–Bernoulli beam model can be obtained by setting the shear strain to zero (namely, $\psi = -v_{,3}$). In doing so, we get the governing equations for bending PS beams without shear deformation

$$\begin{aligned} -(\bar{c}_{33}I + c_{33}^s I^s)v_{,3333} + (\bar{e}_{33}I + e_{33}^s I^s)\varphi_{,333}^{(1)} &= \rho A \ddot{v}, \\ -\bar{e}_{33}Iv_{,333} - \bar{\epsilon}_{33}I\varphi_{,33}^{(1)} + \bar{\epsilon}_{11}A\varphi^{(1)} &= -qIn^{(1)}, \\ -n_0\mu_{33}^n I\varphi_{,33}^{(1)} + D_{33}^n In_{,33}^{(1)} + n_0\mu_{11}^n A\varphi^{(1)} - D_{11}^n An^{(1)} &= In^{(1)}. \end{aligned} \tag{17}$$

In this case, the equivalent bending moment and shear force, and the resultant electric displacements are

$$\begin{aligned} M^* &= -(\bar{c}_{33}I + c_{33}^s I^s)v_{,33} + (\bar{e}_{33}I + e_{33}^s I^s)\varphi_{,3}^{(1)}, \\ Q^* &= -(\bar{c}_{33}I + c_{33}^s I^s)v_{,333} + (\bar{e}_{33}I + e_{33}^s I^s)\varphi_{,33}^{(1)}, \\ D_2^{(0)} &= -\bar{\epsilon}_{11}A\varphi^{(1)}, \\ D_3^{(1)} &= -\bar{e}_{33}Iv_{,33} - \bar{\epsilon}_{33}I\varphi_{,3}^{(1)}. \end{aligned} \tag{18}$$

Static bending analysis of PS beams under a uniform distributed load

Consider a simply supported PS beam under static uniform distributed load q_0 . The considered PS beam is with open-circuit and electrically isolated boundary conditions at the two ends. For the static bending of PS beams, the 1D governing equations become

$$\begin{aligned} -(\bar{c}_{33}I + \pi R^3 c_{33}^s)v_{,3333} + (\bar{e}_{33}I + \pi R^3 e_{33}^s)\varphi_{,333}^{(1)} &= q_0, \\ -\bar{e}_{33}Iv_{,333} - \bar{\epsilon}_{33}I\varphi_{,33}^{(1)} + \bar{\epsilon}_{11}A\varphi^{(1)} &= -qIn^{(1)}, \\ -n_0\mu_{33}^n I\varphi_{,33}^{(1)} + D_{33}^n In_{,33}^{(1)} + n_0\mu_{11}^n A\varphi^{(1)} - D_{11}^n An^{(1)} &= 0. \end{aligned} \tag{19}$$

For the simply supported PS beam with open-circuit and electrically isolated boundary conditions at the two ends ($x_3 = 0, L$), there are

$$\begin{aligned} v(0) &= v(L) = 0, \\ M(0) &= M(L) = 0, \\ D_3^{(1)}(0) &= D_3^{(1)}(L) = 0, \\ J_3^{n(1)}(0) &= J_3^{n(1)}(L) = 0. \end{aligned} \tag{20}$$

Equations (19) and (20) constitute a common boundary value problem of partial differential equations. The basic physical quantities $v, \varphi^{(1)}$, and $n^{(1)}$ can be solved as

$$\begin{aligned} v &= \frac{f_0}{\beta} (C_1 \sinh \beta x_3 + C_2 \cosh \beta x_3) - f_1 \left(\frac{q_0}{24} x_3^4 + \frac{C_0}{6} x_3^3 \right) + C_3 x_3^2 + C_4 x_3 + C_5, \\ \varphi^{(1)} &= C_1 \cosh \beta x_3 + C_2 \sinh \beta x_3 - f_2 \frac{\bar{e}_{33}}{q\bar{\epsilon}_{33}} (C_0 + q_0 x_3), \\ n^{(1)} &= \frac{n_0 q}{kT} \varphi^{(1)}. \end{aligned} \tag{21}$$

In Eq. (21)

$$\begin{aligned} C_0 &= -\frac{q_0 L}{2}, \quad C_1 = 2 \frac{(1 - \cosh \beta L)}{\beta \sinh \beta L} \frac{\bar{e}_{33}}{\bar{\epsilon}_{33}} f_2, \\ C_2 &= \frac{\bar{e}_{33} f_2}{\bar{\epsilon}_{33} \beta}, \quad C_3 = \frac{f_2 f_0 \bar{e}_{33}}{2 \bar{\epsilon}_{33}}, \\ C_4 &= -f_0 f_2 \frac{\bar{e}_{33}}{\bar{\epsilon}_{33}} \left(\frac{1 - \cosh \beta L}{\beta^2 L} + \frac{L}{2} \right) - \frac{q_0 f_3 L^3}{24}, \quad C_5 = -\frac{f_0 f_2 \bar{e}_{33}}{\lambda_3^2 \bar{\epsilon}_{33}}, \\ f_0 &= \frac{\bar{e}_{33} I + e_{33}^s I^s}{\bar{c}_{33} I + c_{33}^s I^s}, \quad f_1 = \frac{1}{\bar{c}_{33} I + c_{33}^s I^s}, \\ f_2 &= \frac{\bar{e}_{33} q_0}{\left(\bar{\epsilon}_{11} \frac{A}{I} + \frac{n_0 q^2}{kT} \right) (\bar{c}_{33} + c_{33}^s I^s / I)}, \quad \beta = \sqrt{\left(\bar{\epsilon}_{11} \frac{A}{I} + \frac{n_0 q^2}{kT} \right) / (\bar{e}_{33} f_0 + \bar{\epsilon}_{33})}. \end{aligned}$$

In addition, from Eq. (19) we can obtain the effective flexural rigidity of $[EI]_s = \left(\bar{c}_{33} + \frac{\bar{e}_{33}^2}{\bar{\epsilon}_{33}}\right)I + \left(c_{33}^s + \frac{\bar{e}_{33}e_{33}^s}{\bar{\epsilon}_{33}}\right)I^s$ of the considered PS beam through writing the bending equation in terms of the deflection v . The first term $\left(\bar{c}_{33} + \frac{\bar{e}_{33}^2}{\bar{\epsilon}_{33}}\right)I$ denoted by $[EI]_0$ represents the classical flexural rigidity of PS beams without considering surface effects. The second term resulting from the surface part plays a dominant role at nanoscale, while is negligible at macroscale.

Free bending vibration of a simply supported PS beam

In this section, consider the free bending vibration of a simply supported PS beam. Strictly speaking, it is a damped free vibration resulting from the motion of carriers. Assume the following solutions [25], satisfying with the boundary conditions of Eq. (20), as

$$\begin{aligned} v &= A_1 \sin k_m x_3 q(t), \\ \varphi^{(1)} &= A_2 \cos k_m x_3 q(t), \\ n^{(1)} &= A_3 \cos k_m x_3 q(t), \end{aligned} \tag{22}$$

where $A_1, A_2,$ and A_3 are unknown constants, $k_m = m\pi/L$ ($m = 1, 2, 3, \dots$), $q(t) = \exp(\lambda t)$ reflects the oscillation behavior of the considered PS beam. The substitution of Eq. (22) into Eq. (17), yields

$$\begin{bmatrix} \bar{e}_{33}k_m^3 & \bar{e}_{33}k_m^2 + \bar{\epsilon}_{11}c & q \\ 0 & n_0(\mu_{33}^n k_m^2 + \mu_{11}^n c) & -(D_{33}^n k_m^2 + D_{11}^n c + \lambda) \\ -(\bar{c}_{33} + c_{33}^s cR)k_m^4 - \rho c \lambda^2 & (\bar{e}_{33} + cR e_{33}^s)k_m^3 & 0 \end{bmatrix} \begin{bmatrix} A_1 \\ A_2 \\ A_3 \end{bmatrix} = \begin{bmatrix} 0 \\ 0 \\ 0 \end{bmatrix}. \tag{23}$$

The existence of a nontrivial solution requires that the determinant of coefficient matrix of Eq. (23) must be zero. This yields the following characteristic equation:

$$a_0 \lambda^3 + a_1 \lambda^2 + a_2 \lambda + a_3 = 0, \tag{24}$$

where

$$\begin{aligned} a_0 &= \rho \frac{1}{c} \left(\frac{k_m^2 \bar{e}_{33}}{c} + \bar{\epsilon}_{11} \right), c = A/I, \\ a_1 &= \rho \left(\frac{k_m^2 \bar{e}_{33}}{c} + \bar{\epsilon}_{11} + \frac{qn_0 \mu_{33}^n}{cD_{33}^n} \right) \left(\frac{k_m^2 D_{33}^n}{c} + D_{11}^n \right), \\ a_2 &= \bar{e}_{33} \left(\bar{e}_{33} + \frac{4e_{33}^s}{R} \right) \frac{k_m^6}{c^3} + \left(\frac{k_m^2 \bar{e}_{33}}{c} + \bar{\epsilon}_{11} \right) \left(\bar{c}_{33} + \frac{4c_{33}^s}{R} \right) \frac{k_m^4}{c^2}, \\ a_3 &= \bar{e}_{33} \left(\bar{e}_{33} + \frac{4e_{33}^s}{R} \right) \left(\frac{k_m^2 D_{33}^n}{c} + D_{11}^n \right) \frac{k_m^6}{c^2} \\ &+ \left(\frac{k_m^2 \bar{e}_{33}}{c} + \bar{\epsilon}_{11} + \frac{qn_0 \mu_{33}^n}{cD_{33}^n} \right) \left(\bar{c}_{33} + \frac{4c_{33}^s}{R} \right) \left(\frac{k_m^2 D_{33}^n}{c} + D_{11}^n \right) \frac{k_m^4}{c}. \end{aligned} \tag{25}$$

In Eq. (25), a_1 and a_3 contain material constants related to semiconductor properties, while a_0 and a_2 do not. For the case of pure piezoelectric beams, both a_1 and a_3 are zeros in Eq. (25), and thus, the characteristic equation of Eq. (24) becomes

$$(a_0 \lambda^2 + a_2) \lambda = 0. \tag{26}$$

We immediately have

$$\lambda_1 = 0, \lambda_{2,3} = \pm i \sqrt{a_2/a_0}. \tag{27}$$

The zero root λ_1 has no physical meaning and is thus omitted. Accordingly, the general solution of $q(t)$ is

$$q(t) = B_1 \cos \omega_m t + B_2 \sin \omega_m t. \tag{28}$$

B_1 and B_2 are unknown constants and dependent on the initial condition. The m th-order natural frequency ω_m is given as

$$\omega_m = \text{Im}[\lambda_2] = \sqrt{a_2/a_0} = k_m^2 \sqrt{\frac{1}{\rho c} \sqrt{\bar{c}_{33} + \frac{4c_{33}^s}{R} + \frac{\bar{e}_{33}(\bar{e}_{33} + 4e_{33}^s/R)}{\bar{\epsilon}_{33} + c\bar{\epsilon}_{11}/k_m^2}}}. \tag{29}$$

In Eq. (29), by getting rid of corresponding material constants, we can directly obtain the natural frequencies for piezoelectric (${}^s\omega_m^{PE}$) and pure elastic (${}^s\omega_m^E$) beams with considering surface effects, and those for piezoelectric (ω_m^{PE}) and pure elastic beams (ω_m^E) beams without considering surface effects. They are

$$\begin{aligned} {}^s\omega_m^{PE} &= {}^s\omega_m^E \sqrt{1 + {}^s k_{33}^{-2} \left(1 + \frac{c\bar{\epsilon}_{11}}{\bar{\epsilon}_{33}k_m^2}\right)^{-1}}, & {}^s\omega_m^E &= \omega_m^E \sqrt{1 + \frac{4c_{33}^s}{\bar{c}_{33}R}}, \\ \omega_m^{PE} &= \omega_m^E \sqrt{1 + k_{33}^{-2} \left(1 + \frac{c\bar{\epsilon}_{11}}{\bar{\epsilon}_{33}k_m^2}\right)^{-1}}, & \omega_m^E &= k_m^2 \sqrt{\frac{\bar{c}_{33}}{c\rho}}. \end{aligned} \tag{30}$$

In Eq. (30), ${}^s\bar{k}_{33} = \bar{k}_{33} \sqrt{\left(1 + \frac{4e_{33}^s}{\bar{\epsilon}_{33}R}\right)\left(1 + \frac{4c_{33}^s}{\bar{c}_{33}}\right)^{-1}}$ and $\bar{k}_{33} = \sqrt{\frac{\bar{e}_{33}^2}{\bar{c}_{33}\bar{\epsilon}_{33}}}$ represent the electromechanical coupling coefficients of piezoelectric beams with and without considering surface effects. Equation (30) implies that both piezoelectricity and surface effects tend to increase the natural frequencies of structures. This is because they increase the effective flexural rigidity of PS beams. Note that the surface effect maybe increases or decreases natural frequencies of PS beams when considering surface positive or negative residual stresses.

Next, we solve the characteristic equation [Eq. (24)] for PS beams. The motion of carriers inside PSs plays a fundamental role in semiconductor devices. However, the motion of carriers can cause a damping effect in the bending vibration of PS beams at the same time. The three roots (λ_1, λ_2 , and λ_3) of the characteristic equation Eq. (24) can be obtained in terms of Cardan’s formula

$$\begin{aligned} \lambda_1 &= -\frac{a_1}{3a_0} + Y_1^{\frac{1}{3}} + Y_2^{\frac{1}{3}}, \\ \lambda_{2,3} &= -\frac{a_1}{3a_0} - \frac{1}{2}(Y_1^{\frac{1}{3}} + Y_2^{\frac{1}{3}}) \pm i\frac{\sqrt{3}}{2}(Y_1^{\frac{1}{3}} - Y_2^{\frac{1}{3}}), \end{aligned} \tag{31}$$

where $Y_{1,2} = -\frac{p_2}{2} \pm \sqrt{\left(\frac{p_2}{2}\right)^2 + \left(\frac{p_1}{3}\right)^3}$, $p_1 = \frac{3a_0a_2 - a_1^2}{3a_0^2}$, and $p_2 = \frac{27a_0^2a_3 - 9a_0a_1a_2 + 2a_1^3}{27a_0^3}$. When $\Delta = \left(\frac{p_2}{2}\right)^2 + \left(\frac{p_1}{3}\right)^3$ is positive, there are one real root λ_1 and two complex conjugate roots $\lambda_{2,3}$. For the considered PS beam in this paper, Δ is always positive, which is numerically shown in **Appendix I**. In this case, the oscillation motion $q(t)$ can be written as in the form of

$$q(t) = B_1 e^{-\zeta_{1m}\omega_m t} + e^{-\zeta_{2m}\omega_m t} (B_2 \cos \omega_m^d t + B_3 \sin \omega_m^d t). \tag{32}$$

In Eq. (32), there are $\zeta_{1m} = -\lambda_1/\omega_m$ and $\zeta_{2m} = -\text{Re}[\lambda_2]/\omega_m$, the expression of ω_m has been given as ${}^s\omega_m^{PE}$ in Eq. (30). $\omega_m^d = \text{Im}[\lambda_2] = \frac{\sqrt{3}}{2}(Y_1^{\frac{1}{3}} - Y_2^{\frac{1}{3}})$ represents natural frequencies of damped free bending vibration of PS

beams. In Eq. (32), both $e^{-\zeta_{1m}\omega_m t}$ and $e^{-\zeta_{2m}\omega_m t}$ are exponentially decaying functions of time. The first term $B_1 e^{-\zeta_{1m}\omega_m t}$ indicates a rapidly decaying motion without oscillation corresponding to the overdamped case of classical vibration theory [56]. For the considered problem, ζ_{1m} is far larger than ζ_{2m} which can be shown in Fig. 11 (see Sect. 6). Actually, it is not possible that the motion of carriers produces such a “huge” damping effect in the free bending vibration of PS beams. Hence, $B_1 e^{-\zeta_{1m}\omega_m t}$ should be deleted, namely, we have

$$q(t) = e^{-\zeta_{2m}\omega_m t} (B_2 \cos \omega_m^d t + B_3 \sin \omega_m^d t). \tag{33}$$

The two unknown constants B_2 and B_3 can be determined from initial conditions. To make a representation of $q(t)$, without loss generality, we assume initial conditions with $q(0) = Q_0$ and $\dot{q}(0) = Q_1$. Substituting them into Eq. (33), we get $B_2 = Q_0$ and $B_3 = (\zeta_{2m}\omega_m Q_0 + Q_1)/\omega_m^d$, and then

$$q(t) = \sqrt{B_2^2 + B_3^2} e^{-\zeta_{2m}\omega_m t} \sin(\omega_m^d t + \Phi), \tag{34}$$

where $\Phi = \arctan [Q_0\omega_m^d / (\zeta_{2m}\omega_m Q_0 + Q_1)]$. Following the similar approach as in Ref. [58], we can evaluate the rate of decay of free oscillations of PS beams through computing the natural logarithm of the ratio of any two successive amplitudes, that is

$$\delta = \ln \frac{q(t_1)}{q(t_1 + \tau_d)} = \zeta_{2m}\omega_m \tau_d. \tag{35}$$

$\tau_d = 2\pi/\omega_m^d$ is the damped period. In addition, we define the decay time t_{decay} as the period of the amplitude

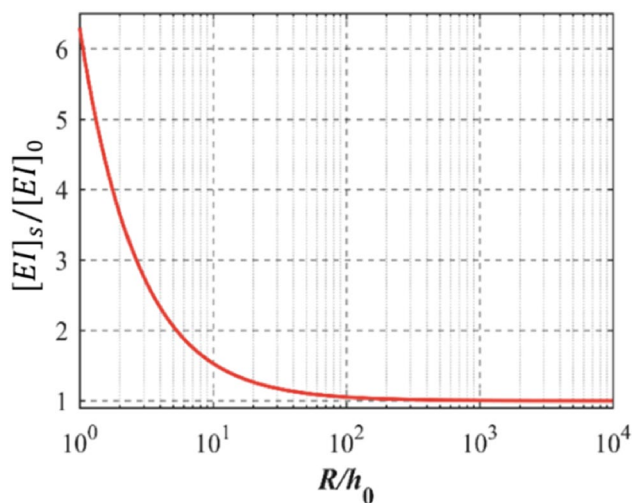


Fig. 3 Normalized effective flexural rigidity $[EI]_s/[EI]_0 = 1 + \frac{h_0}{R} \frac{c_{33}\bar{\epsilon}_{33} + \bar{e}_{33}^2}{\bar{c}_{33}\bar{\epsilon}_{33} + \bar{e}_{33}^2}$

Fig. 4 Distributions of electromechanical fields at $x_2=R$: **a** deflection v , **b** potential φ , **c** incremental carrier concentrations Δn ($L=600$ nm, $R=30$ nm, $n_0=10^{23}$ m $^{-3}$)

$\sqrt{Q_0^2+Q_1^2}e^{-\zeta_{2m}\omega_m t}$ decaying by a factor of $1/e$. Then, we have

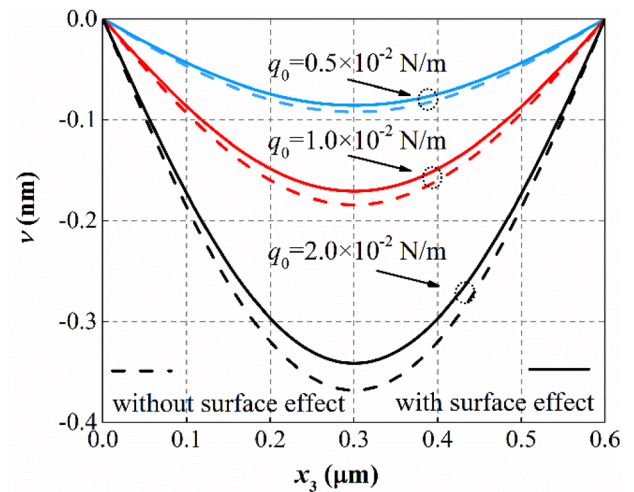
$$t_{decay} = 1/\zeta_{2m}\omega_m. \quad (36)$$

Numerical examples and discussion

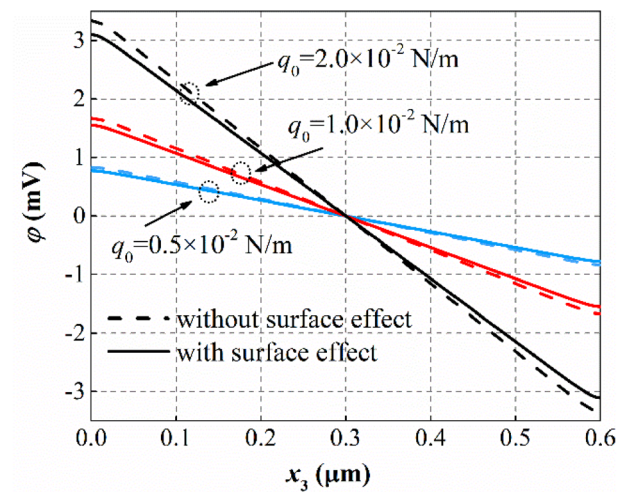
In this section, we use the derived theoretical model to numerically study the static bending and free vibration of a simply supported beam made of n-type ZnO. As numerical examples, the length of the beam and the radius of cross-section are chosen as $L=600$ nm and $R=30$ nm, and the initial electron concentration is $n_0=10^{23}$ m $^{-3}$. The materials constants of the bulk ZnO are from Ref. [55]. For the sake of simplicity, we adopt the same feasible and reasonable method as in Ref. [47] for the surface material constants f_s , that is, they are proportional to its bulk counterpart f_B . The scale factor is equivalent to the intrinsic material length h_0 . Namely, $f_s \approx f_B h_0$. According to Ref. [59], the intrinsic material length of ZnO is chosen as $h_0=0.4$ nm in this paper.

First, consider the static bending of the PS beam under different uniform distributed forces ($q_0=0.5, 1.0,$ and 2×10^{-2} N/m) per unit width. With the analytical solutions obtained in Sect. 4, we can evaluate the effective flexural rigidity $[EI]_s$, deflection v , electric potential φ , and incremental concentration of electrons Δn along the PS beam. Figure 3 shows the size-dependent characteristics of $[EI]_s$ normalized by $[EI]_0$. It can be observed that the surface effect almost has no effect when R/h_0 is greater than 100 or so (namely, the radius of the beam is larger than about 400 nm); however, it brings a dramatic change of the effective flexural rigidity $[EI]_s$ when R is smaller than 400 nm. For example, $[EI]_s$ increases from $1.1[EI]_0$ to $1.6[EI]_0$ with R decreasing from 400 to 40 nm. Such a phenomenon attributed to the surface effect can be called the surface-induced stiffening effect, similar to the piezoelectric stiffening effect.

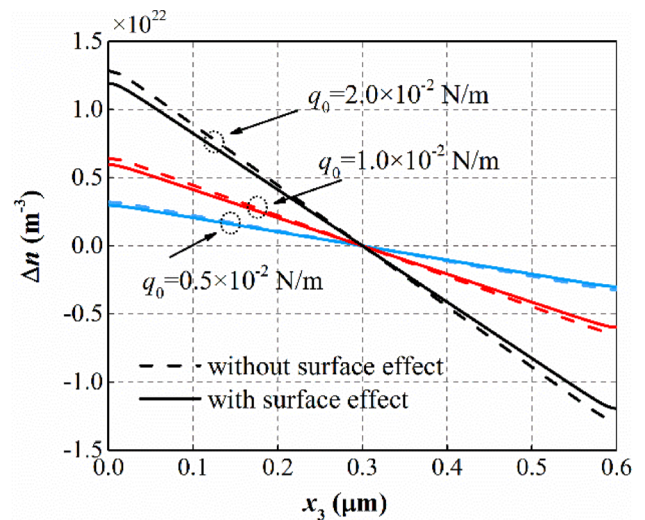
Figures 4 shows the distribution of v , $\varphi=R\varphi^{(1)}$, and $\Delta n=Rn^{(1)}$ along the beam at $x_2=R$ without/with considering surface effects. It can be observed that for the considered PS beam, the surface effect plays a decreasing role in the mechanical and electrical responses of the PS beam due to the surface-induced stiffening effect. For example, the surface effect lowers the amplitude of v , φ , and Δn . The electrical potential displays an almost linear and anti-symmetric distribution along its axial direction (x_3) of the PS beam, as shown in Fig. 4b. It can be seen, from Fig. 4c that the



(a)



(b)



(c)

Fig. 5 The first-order normalized natural frequencies for different initial concentrations of electrons: **a** without and **b** with surface effects ($L=600$ nm, $R=30$ nm)

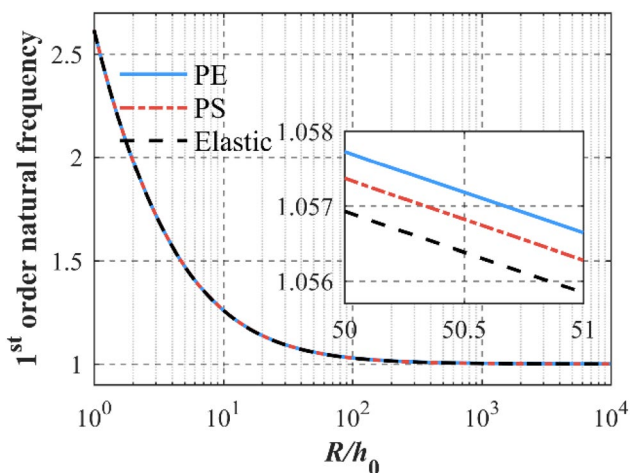
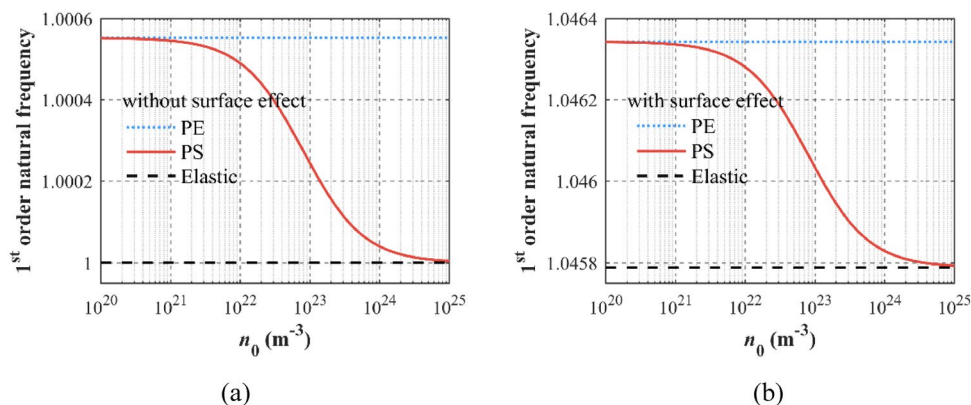


Fig. 6 The 1st-order normalized natural frequencies under different values of R/h_0 with $L/R=20$

distribution of Δn exhibits the same trend as the electric potential. This is because of the electrons redistributing itself driven by the induced piezoelectric potential. The electrons have a larger variation in the two ends.

Next, consider the free bending vibration of the PS beam with the same geometrical size as it in the preceding

example. Based on the analytical expressions derived in Sect. 5, we set $m=1$ to evaluate the first-order natural frequencies of the PS beam under different initial concentrations. Meanwhile, the first-order natural frequencies for piezoelectric and elastic beams with the same geometrical size are also provided. These frequencies normalized by ω_1^E are plotted in Fig. 5. The symbols of ‘PS’, ‘PE’, and ‘Elastic’ appeared in Figs. 5 and 6 denote the cases of piezoelectric semiconductor, piezoelectric, and elastic beam, respectively. From Fig. 5, we find that the surface effect makes the natural frequencies a significant increase. For different initial electron concentrations n_0 , the first-order natural frequencies of the PS beam are always larger than those of pure elastic beams, while are smaller than ones of piezoelectric beams. Only the initial concentration of electrons ranging from 10^{22} m^{-3} to 10^{24} m^{-3} plays a tuning role in the natural frequencies of PS beams.

To get a deeper understanding of size-dependent properties of the considered bending PS beam due to surface effects, we calculate the first-order natural frequencies for different values of R/h_0 when $n_0=10^{23}$ m^{-3} , the ratio of $L/R=20$, and $h_0=0.4$ nm are fixed. Figure 6 shows the size-dependent property of the 1st-order natural frequency of the PS beam. With the reduction of R , the surface effect makes the first-order natural frequency a dramatic rise. This

Fig. 7 **a** ζ_1 , and **b** ζ_2 for different initial concentrations of electrons ($L=600$ nm, $R=30$ nm)

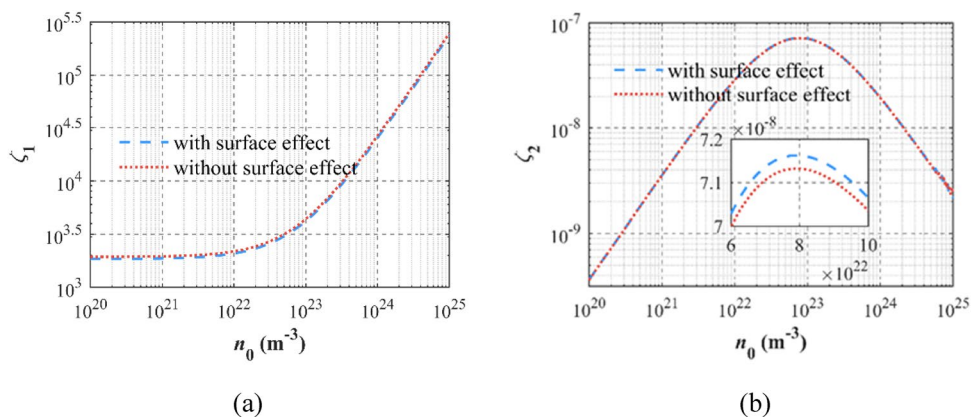


Fig. 8 Amplitude of $q(t)$ versus time t : **a** without surface effects and **b** with surface effects for different initial concentration of electrons n_0 ($L=600$ nm, $R=30$ nm)

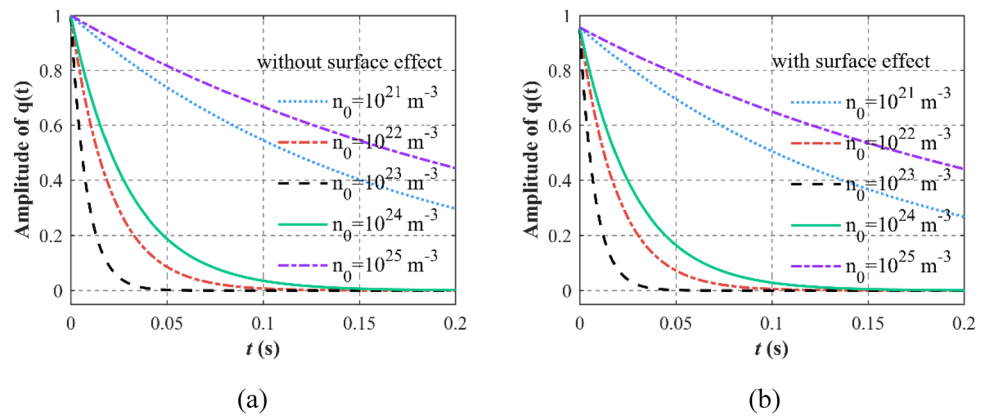
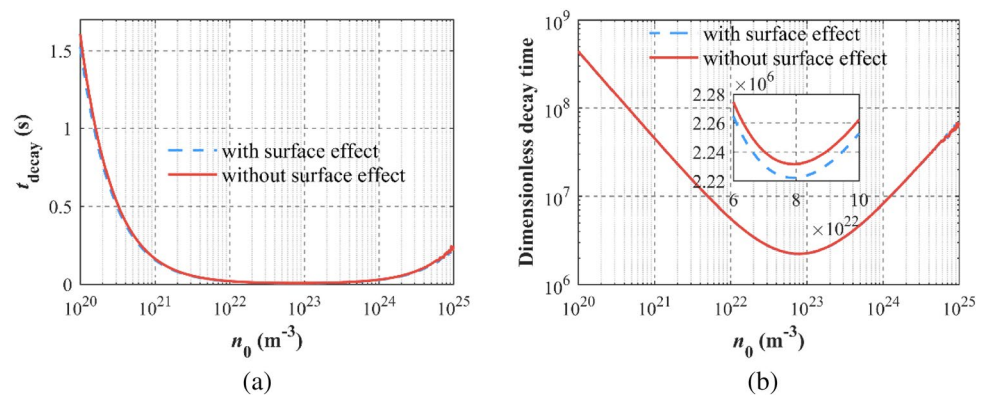


Fig. 9 **a** Decay time and **b** dimensionless decay time under different initial concentrations of electrons ($L=600$ nm, $R=30$ nm)



is because of the surface-induced stiffening effect. The surface effect should be taken into consideration when the value of R/h_0 decreases to about 400 for the considered PS beam.

It is the motion of carriers that produces a damping force for the vibration of PS beams. Such a damping effect mainly depends on the total amount of carriers. We compute the quasi-damping ratio ζ_2 for different initial concentrations of electrons, and the value of ζ_1 is also evaluated. The curves of ζ_1 and ζ_2 under different initial concentrations of electrons are plotted in Fig. 7. It can be observed from Fig. 7 that ζ_1 is more than 10 orders of magnitude larger than ζ_2 . Figure 7b shows the quasi-damping ratio ζ_2 increases from zero to its maximum 7.15×10^{-8} with n_0 increasing to about $8 \times 10^{22} \text{ m}^{-3}$, and then, ζ_2 decreases sharply with the increase of n_0 . The quasi-damping ratio ζ_2 with surface effects is larger than those without surface effects.

Figure 8 shows the decay behavior of the oscillatory amplitude of $q(t)$ for different initial concentrations of electrons without and with considering surface effects. The initial concentration of electrons has an important effect on the decaying of the oscillatory amplitude of $q(t)$. This is because the value of quasi-damping ratio ζ_2 is dependent

on the initial concentration of electrons. To represent the dependent relation of the decay time on the initial concentration of electrons in detail, we plot the decay time and the normalized decay time by $2\pi/\omega_d$ under different initial concentrations of electrons in Fig. 9. It can be seen that the considered PS beam undergoes a faster-attenuating oscillation when $n_0 \in (10^{22}, 10^{24})$.

Conclusions

In summary, based on the G-M surface theory, we treat the surface effect as a non-classical boundary condition and develop the 1D deformation-polarization-carrier coupling model for beam-like PS nanostructures with arbitrary cross-section. The derived equations are useful for studying the bending of PS beams at nanoscale. Both the static bending and free vibration analysis of a simply supported n-type PS beam with open circuit and electrically isolated boundary conditions are investigated. For the static bending of the PS beam under the uniform distributed load q_0 , the analytical solutions of the effective flexural rigidity, deflection,

potential, and incremental concentration of electrons are presented. For the free vibration of the PS beam, the analytical expressions of natural frequencies and the carriers-induced damping effect are presented. Such a damping effect due to the motion of carriers depends on the initial concentration of electrons. The initial concentration of electrons ranging from 10^{22} m^{-3} to 10^{24} m^{-3} leads to a strong damping effect. The surface effect has a remarkable effect on the effective flexural rigidity and natural frequencies of the bending PS beam. The initial concentration of electrons plays a role in the natural frequencies and oscillation motion of the bending PS beam. The numerical results are helpful to understand multi-field coupling behaviors of PS nanostructures, and in designing PS nanodevices, as well.

Appendix I: Numerical values of Δ

In Eq. (31), the three roots λ_1 , λ_2 , and λ_3 are available when

$$\Delta = \left(\frac{p_2}{2}\right)^2 + \left(\frac{p_1}{3}\right)^3 > 0. \quad (\text{A1})$$

The material and geometrical constants of the ZnO PS beam have been given in Sect. 6. We evaluate Δ under different initial concentrations of electrons and plot it in Fig. 10. It can be seen that Δ is always positive and has a very large value.

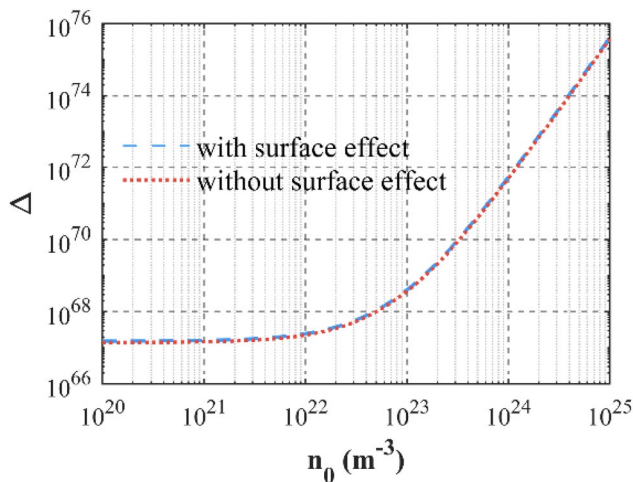


Fig. 10 Δ in Eq. (A1) for different initial concentrations of electrons. ($L=600 \text{ nm}$, $R=30 \text{ nm}$)

Acknowledgements This work was supported by the National Natural Science Foundation of China (Nos. 11972139 and 11672265), Natural Science Foundation of Zhejiang province, China (No. LY18A020006), the National Key Research and Development Program of China (No. 2020YFA0711701), and the State Key Laboratory of Mechanics and Control of Mechanical Structures (Nanjing University of Aeronautics and astronautics, No. MCMS-E-0220K01).

References

1. Wang ZL (2007) Nanopiezotronics. *Adv Mater* 19(6):889–892
2. Wang ZL, Wu WZ (2014) Piezotronics and piezo-phototronics: Fundamentals and applications. *Natl Sci Rev* 1(1):62–90
3. Liu Y, Zhang Y, Yang Q et al (2015) Fundamental theories of piezotronics and piezo-phototronics. *Nano Energy* 14:257–275
4. Wang ZL (2012) *Piezotronics and Piezo-Phototronics*. Science Press, Beijing
5. Wang ZL (2004) Zinc oxide nanostructures: growth, properties and applications. *J Phys Condensed Mater* 16(25):R829–R858
6. Wang ZL, Song JH (2006) Piezoelectric nanogenerators based on zinc oxide nanowire arrays. *Science* 312(5771):242–246
7. Cha SN, Seo JS, Kim SM et al (2010) Sound-driven piezoelectric nanowire-based nanogenerators. *Adv Mater* 22(42):4726–4730
8. Park HK, Lee KY, Seo JS et al (2011) Charge-generating mode control in high-performance transparent flexible piezoelectric nanogenerators. *Adv Func Mater* 21(6):1187–1193
9. Fei P, Yeh PH, Zhou J et al (2009) Piezoelectric potential gated field-effect transistor based on a free-standing ZnO wire. *Nano Lett* 9(10):3435–3439
10. Wang XD, Zhou J, Song JH et al (2006) Piezoelectric field effect transistor and nanoforce sensor based on a single ZnO nanowire. *Nano Lett* 6(12):2768–2772
11. Zhou J, Gu YD, Fei P et al (2008) Flexible piezotronic strain sensor. *Nano Lett* 8(9):3035–3040
12. Wu JM, Chen CY, Zhang Y et al (2012) Ultrahigh sensitive piezotronic strain sensors based on a ZnSnO₃ nanowire/microwire. *ACS Nano* 6(5):4369–4374
13. Galstyan V, Comini E, Baratto C et al (2015) Nanostructured ZnO chemical gas sensors. *Ceram Int* 41(10):14239–14244
14. Zhu L, Zeng W (2017) Room-temperature gas sensing of ZnO-based gas sensor: A review. *Sens Actuators A-Phys* 267:242–261
15. Ismail AS, Mamat MH, Rusop M (2015) Humidity sensor: A review of nanostructured zinc oxide (ZnO)-based humidity sensor. *Appl Mech Mater* 773–774:706–710
16. Park JY, Choi SW, Kim SS (2010) Fabrication of a highly sensitive chemical sensor based on ZnO nanorod Arrays. *Nanoscale Res Lett* 5(2):353–359
17. Zhang CL, Wang XY, Chen WQ, Yang JS (2017) An analysis of the extension of a ZnO piezoelectric semiconductor nanofiber under an axial force. *Smart Mater Struct* 26(2):025030
18. Wang GL, Liu JX, Liu XL et al (2018) Extensional vibration characteristics and screening of polarization charges in a ZnO piezoelectric semiconductor nanofiber. *J Appl Phys* 124(9):094502
19. Gao Y, Wang ZL (2007) Electrostatic potential in a bent piezoelectric nanowire. The fundamental theory of nanogenerator and nanopiezotronics. *Nano Lett* 7(8):2499–2505
20. Zhang CL, Wang XY, Chen WQ, Yang JS (2018). Bending of a cantilever piezoelectric semiconductor fiber under an end force ‘Generalized Models and Non-Classical Approaches in Complex

- Materials' Springer Special Volume in Honor of the Memory of Gérard Maugin, editors: Altenbach H et al (Cham, Switzerland: Springer), pp 261–278
21. Fan SQ, Liang YX, Xie JM, Hu YT (2017) Exact solutions to the electromechanical quantities inside a statically-bent circular ZnO nanowire by taking into account both the piezoelectric property and the semiconducting performance: part I-Linearized analysis. *Nano Energy* 40:82–87
 22. Dai XY, Zhu F, Qian ZH, Yang JS (2018) Electric potential and carrier distribution in a piezoelectric semiconductor nanowire in time-harmonic bending vibration. *Nano Energy* 43:22–28
 23. Liang YX, Yang WL, Yang JS (2019) Transient bending vibration of a piezoelectric semiconductor nanofiber under a suddenly applied shear force. *Acta Mech Solid Sin* 32(6):688–697
 24. Yang WL, Hu YT, Yang JS (2019) Transient extensional vibration in a ZnO piezoelectric semiconductor nanofiber under a suddenly applied end force. *Mater Res Express* 6:025902
 25. Romano G, Mantini G, Di Carlo A et al (2011) Piezoelectric potential in vertically aligned nanowires for high output nanogenerators. *Nanotechnology* 22(46):465401
 26. Liang C, Zhang CL, Chen WQ, Yang JS (2019) Static buckling of piezoelectric semiconductor fibers. *Mater Res Express* 6:125919
 27. Huang HY, Qian ZH, Yang JS (2019) I-V characteristics of a piezoelectric semiconductor nanofiber under local tensile/compressive stress. *J Appl Phys* 126:164902
 28. Cheng RR, Zhang CL, Chen WQ, Yang JS (2019) Electrical behaviors of a piezoelectric semiconductor fiber under a local temperature change. *Nano Energy* 66:104081
 29. Cheng RR, Zhang CL, Chen WQ, Yang JS (2018) Piezotronic effects in the extension of a composite fiber of piezoelectric dielectrics and nonpiezoelectric semiconductors. *J Appl Phys* 124(6):064506
 30. Luo YX, Zhang CL, Chen WQ, Yang JS (2018) Piezopotential in a bended composite fiber made of a semiconductive core and of two piezoelectric layers with opposite polarities. *Nano Energy* 54:341–348
 31. Cheng RR, Zhang CL, Zhang Ch, Chen WQ (2020) Magnetically controllable piezotronic responses in a composite semiconductor fiber with multiferroic coupling effects. *Phys Status Solid A* 217:1900621
 32. Yang JS (2005) An anti-plane crack in a piezoelectric semiconductor. *Int J Fract* 136:L27-32
 33. Sladek J, Sladek V, Pan E, Wunsche M (2014) Fracture analysis in piezoelectric semiconductors under a thermal load. *Eng Fract Mech* 126:27–39
 34. Zhao MH, Pan YB, Fan CY, Xu GT (2016) Extended displacement discontinuity method for analysis of cracks in 2D piezoelectric semiconductors. *Int J Solids Struct* 94:50–59
 35. Gu CL, Jin F (2015) Shear-horizontal surface waves in a half-space of piezoelectric semiconductors. *Philos Mag Lett* 95(2):92–100
 36. Jiao FY, Wei PJ, Zhou XL, Zhou YH (2019) The dispersion and attenuation of the multi-physical fields coupled waves in a piezoelectric semiconductor. *Ultrasonics* 92:68–78
 37. Cao XS, Hu SM, Liu JJ, Shi JP (2019) Generalized Rayleigh surface waves in a piezoelectric semiconductor half space. *Meccanica* 54(1–2):271–281
 38. Chen CQ, Shi Y, Zhang YS et al (2006) Size dependence of Young's modulus in ZnO nanowires. *Phys Rev Lett* 96(7):075505
 39. Cao GX, Chen X (2007) Energy analysis of size-dependent elastic properties of ZnO nanofilms using atomistic simulations. *Phys Rev B* 76(16):165407
 40. Gurtin ME, Murdoch AI (1975) A continuum theory of elastic material surfaces. *Arch Ration Mech Anal* 57:291–323
 41. Gurtin ME, Murdoch AI (1978) Surface stress in solids. *Int J Solids Struct* 14:431–440
 42. Lim CW, He LH (2004) Size-dependent nonlinear response of thin elastic films with nano-scale thickness. *Int J Mech Sci* 46:1715–1726
 43. Lu P, He LH, Lee HP, Lu C (2006) Thin plate theory including surface effects. *Int J Solids Struct* 43:4631–4647
 44. Chen WQ, Zhang Ch (2010) Anti-plane shear Green's functions for an isotropic elastic half-space with a material surface. *Int J Solids Struct* 47:1641–1650
 45. Huang GY, Yu SW (2006) Effect of surface piezoelectricity on the electromechanical behaviour of a piezoelectric ring. *Phys Status Solid B* 243(4):R22–R24
 46. Yan Z, Jiang LY (2011) Surface effects on the electromechanical coupling and bending behaviours of piezoelectric nanowires. *J Phys D: Appl Phys* 44:075404
 47. Yan Z, Jiang LY (2012) Surface effects on the electroelastic responses of a thin piezoelectric plate with nanoscale thickness. *J Phys D Appl Phys* 45:255401
 48. Wang GF, Feng XQ (2010) Effect of surface stresses on the vibration and buckling of piezoelectric nanowires. *EPL* 91(5):56007
 49. Yan Z, Jiang LY (2011) The vibrational and buckling behaviors of piezoelectric nanobeams with surface effects. *Nanotechnology* 22:245703
 50. Song HX, Ke LL, Su J et al (2020) Surface effect on the contact problem of a piezoelectric half-plane. *Int J Solids Struct* 185–186:380–393
 51. Zhang CL, Chen WQ, Zhang Ch (2014) Two-dimensional theory of piezoelectric plates considering surface effect. *Eur J Mech A/ Solids* 41:50–57
 52. Wang PY, Li C, Li S (2020) Bending vertically and horizontally of compressive nano-rods subjected to nonlinearly distributed loads using a continuum theoretical approach. *J Vib Eng Technol* 8:947–957
 53. Li HN, Li C, Shen JP, Yao LQ (2021) Vibration analysis of rotating functionally graded piezoelectric nanobeams based on the nonlocal elasticity theory. *J Vib Eng Technol*. <https://doi.org/10.1007/s42417-021-00288-9>
 54. Zhang CL, Zhu J, Chen WQ, Zhang Ch (2014) Two-dimensional theory of piezoelectric shells considering surface effect. *Eur J Mech A/Solids* 43:109–117
 55. Auld BA (1973) *Acoustic fields and waves in solids*, vol 1. Wiley, New York
 56. Pierret RF (1988) *Semiconductor fundamentals*, 2nd edn. Addison-Wesley, Reading, MA
 57. Chen TY, Chiu MS, Weng CN (2006) Derivation of the generalized Young-Laplace equation of curved interfaces in nanoscaled solids. *J Appl Phys* 100(7):074308
 58. Thomson WT, Dahleh MD (2005) *Theory of vibration with applications*, 5th edn. Tsinghua University Press, Beijing
 59. Hadis M, Ümit Ö (2009) *Zinc oxide: fundamentals, materials and device technology*. Wiley, Weinheim

Publisher's Note Springer Nature remains neutral with regard to jurisdictional claims in published maps and institutional affiliations.